


**Acoustic soft metacollimator by broadband digital phase encoding**Erqian Dong<sup>1,2</sup>, Jinhu Zhang,<sup>1</sup> Xiaochun Su<sup>1</sup>, Zhanyuan Gao,<sup>1</sup> Chen Yang,<sup>1</sup> Zhenyu Wang,<sup>3</sup>  
Nicholas X. Fang,<sup>2,\*</sup> and Yu Zhang<sup>1,†</sup><sup>1</sup>*State Key Laboratory of Marine Environmental Science, Key Laboratory of Underwater Acoustic Communication and Marine Information Technology of the Ministry of Education, College of Ocean and Earth Sciences, Xiamen University, Xiamen 361005, China*<sup>2</sup>*Department of Mechanical Engineering, The University of Hong Kong, Hong Kong SAR*<sup>3</sup>*State Key Laboratory of Robotics, Shenyang Institute of Automation, Chinese Academy of Sciences, Shenyang 110016, China* (Received 19 January 2024; revised 8 June 2024; accepted 28 June 2024; published 25 July 2024)

Phase engineering plays a pivotal role in various scientific research and industrial applications including microwaves, optics, and acoustics. However, traditional phase engineering methods lack the flexibility for arbitrary programming due to the absence of digitization. Conversely, while broadband digitization technology holds promise, its utilization in wave engineering has been constrained by narrowband transmission capabilities. In this study, we introduce a novel approach to broadband digital phase encoding spanning frequencies from 50 to 500 kHz. Our methodology is exemplified through the development of an acoustic soft metacollimator with simulations and experiments conducted underwater across different frequency ranges. Our findings demonstrate that the soft metacollimator significantly enhances transmission intensity by 7.7 dB and improves spatial resolution by a factor of 10. Moreover, the soft metacollimator enables novel functionalities such as long-distance energy enhancement and broadband coding properties in underwater acoustics. This pioneering broadband digital phase encoding technique holds promise for advancing next-generation phase engineering and offers versatile applications in biomedical ultrasonics, acoustic communications, and the development of underwater broadband acoustic antennas.

DOI: [10.1103/PhysRevApplied.22.014065](https://doi.org/10.1103/PhysRevApplied.22.014065)**I. INTRODUCTION**

In recent years, the emergence of digital materials has provided us with miniaturized and programmable design methods in microwaves, optics, and acoustics. Metamaterials composed of artificially programmable structures with periodically or nonperiodically arranged subwavelength elements, are designed to exhibit unusual properties beyond those found in natural occurring media. The concept of negative refraction was first proposed as early as the 1960s. Pendry *et al.* introduced a kind of composite structure capable of realizing negative permittivity and permeability at microwave frequencies [1,2]. Subsequently, in 2001, the negative index of refraction was experimentally verified by Shelby *et al.* using periodic metal rods and resonant split rings [3]. With advancements electromagnetic metamaterials (EMs) and ultrasonic metamaterials (UMs) [4–6] have demonstrated

great potential for phase and amplitude control in acoustic fields. They have been applied in many fields such as underwater acoustic communication, passive metasurfaces by phase engineering [7,8], wavefront shaping [9], negative refraction [10], invisible cloaking [11–13], mode transitions [14], acoustic lenses [15], and acoustic holograms [16].

While traditional acoustic metamaterials have made significant progress in freely controlling acoustic waves, their rigid features limit their applications underwater due to impedance mismatch with background medium, limited bandwidth, and significant backscattering characteristics [10,17,18]. Unlike conventional solid materials, soft materials have provided more freedom in designing soft robots [19,20], underwater hydrophones [21], and wearable flexible devices [22,23]. Recent proposed soft metamaterials have been shown to slow down sound speed and elastic modulus by increasing porosity [24]. Furthermore, in underwater acoustics, soft metamaterials exhibit better impedance-matching performance with water than other types of metamaterials, making them better for broadband sound transmission [25,26]. However, previous soft

\*Contact author: [nicxfang@hku.hk](mailto:nicxfang@hku.hk)†Contact author: [yuzhang@xmu.edu.cn](mailto:yuzhang@xmu.edu.cn)

materials with porous structure suffer from scattering loss, and their phase velocity cannot be stable over broadband frequency ranges [27].

Phase encoding technology is widely used in shaping complex wavefronts, including reflected waves [28], transmitted waves [29], and acoustic beam generation [30]. This encoding can be achieved through the resonant phase shift of helical microstructure [31], or the generalized Snell's law [9]. Labyrinth and spiral structure in coiling-up-space acoustics are useful for changing the sound path to control phase [32,33]. However, these structures can only achieve phase shifts in narrow frequency bands and are not suitable for underwater acoustics devices design due to impedance mismatch [33]. Therefore, materials meeting the underwater broadband acoustic characteristics must satisfy two requirements: tunable acoustic parameters and impedance matching with water. Tunable materials can adjust their physical properties through their excitation sources, for example, electromagnetic control, and circulator by motor control [34,35]. Such unique encoding properties may enable distinct abilities in acoustic tweezers [36], high-speed acoustic communication [37] and acoustic hologram [16]. As for impedance-matching, soft materials (such as silicone rubber and hydrogel) may serve as a suitable candidate as impedance-matching materials with water [38,39].

This paper presents an acoustic soft metacollimator by broadband digital phase encoding. By utilizing different volume fractions of the silicone elastomers in water to adjust the effective sound speed, we can manipulate the transmission phase across the range from coding bit "0" to "2 $\pi$ ." This proposed broadband digital phase encoding enables the creation of a soft metacollimator capable of operation at various frequencies. Initially, the digital phase encoding involves nine types of unit cells, each comprising silicone elastomer columns with identical bottom shapes but varying interior volume fractions. By precisely adjusting the filling fraction of the soft elastomer in water, we can assemble an effective sound speed exhibiting a gradient phase deflection in a discrete distribution. Next, we experimentally validated that a flat acoustic phase profile can be transformed to linearly changing phase distributions across frequencies ranging from 100 to 500 kHz. Based on the analysis above, we demonstrated that the designed soft metacollimator, enabled by broadband encoding, effectively manipulates acoustic wavefronts in both simulations and experiments. Notably, encoding the initial phase profile required for achieving acoustic collimation converts omnidirectional sources to collimation beams effectively in both simulations and experiments. Results indicate that the soft metacollimator increases intensity transmission by 7.7 dB and the spatial resolution by a factor of 10. Such broadband phase encoding with high-efficiency transmission holds promise in expanding applications in underwater acoustic and biomedical ultrasonics.

## II. THEORETICAL ANALYSIS OF BROADBAND DIGITAL PHASE ENCODING

We start the point of our design with an arbitrary phase encoding model. In gels and liquids, we may assume that longitudinal waves are the only supported modes of propagation. Therefore, the acoustic wave equation can be written in the time-harmonic form:

$$\nabla[\rho^{-1}(r)\nabla p(r,t)] = \frac{1}{\kappa(r)} \frac{\partial^2 p(r,t)}{\partial t^2}, \quad (1)$$

where  $\kappa(r)$  is the bulk modulus, considering the condition of uniform mass density, the above equation has the formal solution  $p(r,t) = A(r)e^{j(\omega t - k(r)\psi(r))}$ , where  $A$  is the sound pressure amplitude, a function of spatial location.  $k = k_0 n(r)$  is the wavenumber in a nonuniform medium of refractive index, and  $k_0$  is the wavenumber in free space. By introducing the eikonal equation  $\varphi(r) = n(r)\psi(r)$ , the formal solution  $p(r,t) = A(r)e^{j(\omega t - k_0\varphi(r))}$  is introduced into the wave equation (1), where  $\omega$  is the angular frequency. We can derive the real part of the complex analytic function as follows:

$$\frac{\nabla^2 A(r)}{A(r)} - k_0^2 \nabla\varphi(r) \cdot \nabla\varphi(r) + k^2(r) = 0, \quad (2)$$

when  $\nabla A^2/A \ll k^2$ , we can obtain

$$\frac{d}{ds} \nabla\varphi = \nabla n(x,y,z), \quad (3)$$

where  $ds = \sqrt{dx^2 + dy^2 + dz^2}$ . Therefore, the refractive index along the sound propagation direction can be changed by encoding the phase of the sound pressure. The eikonal equation  $\varphi(r)$  can be obtained by linearly superimposed by  $\varphi_1(x,y)$  and  $\varphi_2(z)$ , that is,  $\varphi(r) = \varphi_1(x,y) + \varphi_2(z)$ . The incident angles of sound waves along axis  $x$ ,  $y$ , and  $z$  are  $\alpha$ ,  $\beta$ , and  $\gamma$ , respectively. According to the relationship between the sound pressure phase and the incident angle  $\partial\varphi/\partial x = n \cos \alpha$ ,  $\partial\varphi/\partial y = n \cos \beta$ , and  $\partial\varphi/\partial z = n \cos \gamma$ , where  $\alpha_0$  and  $\beta_0$  are the initial incident angles. Hence, considering the normal incident of acoustic wave  $\alpha_0 = \beta_0 = \pi/2$ . The expression to achieve arbitrary phase encoding is shown as follows:

$$\Psi_t(x,y,z) = k_0 \int_0^z n(x,y,z) dz = k_0 n_{\text{eff}} z \quad (4)$$

where,  $n_{\text{eff}}(x,y) = n_0 + T(x,y)(n_s - n_0)/H$ ,  $n_0$  and  $n_s$  are the refractive index of background medium and substrate,  $T(x,y)$  is the 2D distribution function of the thickness of the substrate,  $H$  represents the maximum height of the substrate. Therefore, we can obtain the transmission phase

profile, as follows:

$$\Psi_i(x, y) = 2\pi \left( \frac{T(x, y)}{\lambda_s} + \frac{H - T(x, y)}{\lambda_0} \right) + \Psi_i, \quad (5)$$

where  $\lambda_s$  and  $\lambda_0$  are wavelengths in the substrate and background medium, respectively, and  $\Psi_i$  is the incident sound pressure phase.

As shown in Fig. 1(a), the incident phase  $\psi_i$  can be controlled in a programmed way via digital phase encoding, the transmission phase is encoded into  $\psi_i + \psi_0$ ,  $\psi_i + 2\psi_0$  . . . and  $\psi_i + n\psi_0$ , where  $n$  represents the steps of digitization, which makes  $\psi_i + n\psi_0 = 2\pi$ . In Fig. 1(b), the soft elastomer with different volume fractions has been released into the 3D printing model with background water to tune the acoustic effective sound speed. The phase encoding mold is made of polylactide with the same total length and width of 126 mm. As shown by its 3D mold view in Fig. 1(b), there are nine discrete phase encoding models on the plate around the center, with the same width  $W$  and variation depth  $T(x, y)$ .

The effective refractive index of silicone elastomer in water gradually decreases from 1.48 to 1 with volume

fraction of  $T(x, y)/H$ . By filling soft silicone elastomer in water with different volume fractions, where the height of total column  $H = 60$  mm, the original flat phase profile is converted into a linear phase profile. As shown in Fig. 1(c), the transmission phase is encoded by the phase encoding model as the coding bit “0,” “ $\pi/4$ ,” “ $\pi/2$ ,” “ $3\pi/4$ ,” “ $\pi$ ,” “ $5\pi/4$ ,” “ $3\pi/2$ ,” “ $7\pi/4$ ,” and “ $2\pi$ ,” respectively. Since the diameter of the plane wave generator is 125 mm, we set up three different types of phase encoding models along  $x$  and  $y$  directions with the same width  $W = 42$  mm. The fabrication method of phase encoding is presented in the Supplementary Material [40]. The thickness of the ABS mold is  $\Delta h = 3$  mm. With the increasing digitization steps, the theoretical phase shift curves are shown in Fig. 1(d). In the actual process of discretization, the continuous phase distribution is digitized into discrete units of different orders. Here, the segmentation results of a continuous phase profile are shown for 5-step digitization, 9-step digitization, and 21-step digitization. Among them, under the same horizontal and vertical dimension conditions, the pixel unit density increases with the increase of the digitization rate, while the width of each pixel unit gradually decreases. Next, we need to experimentally verify that the

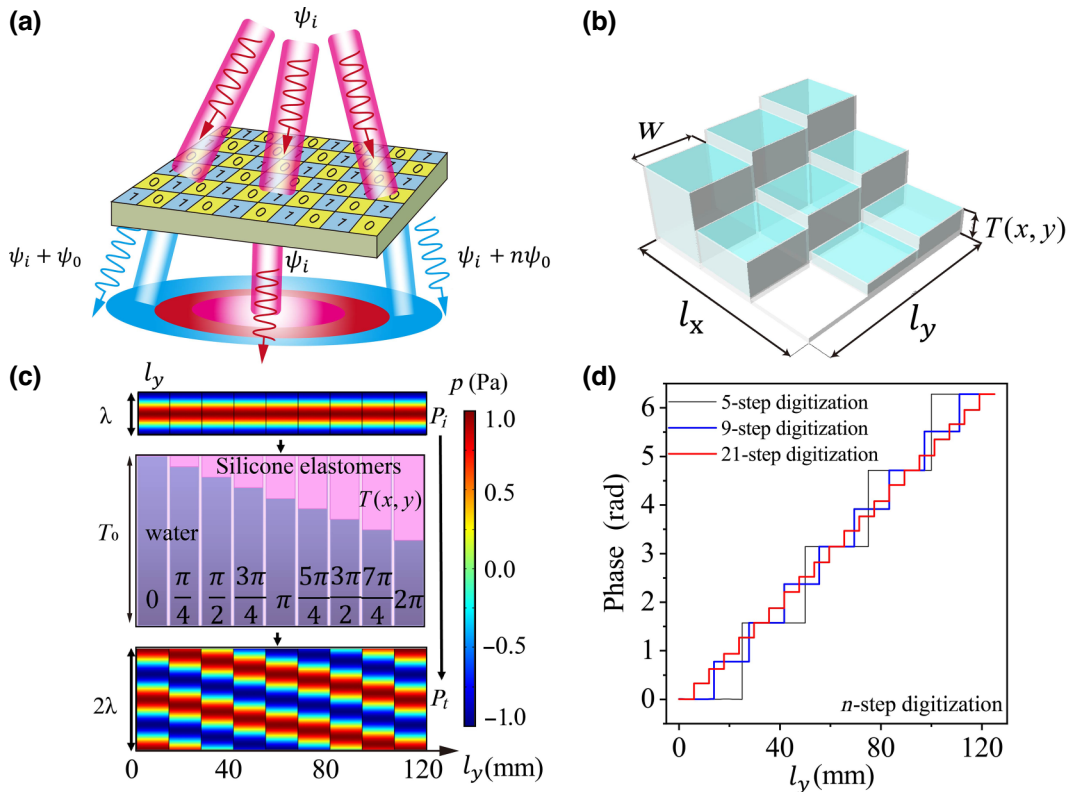


FIG. 1. (a) Schematic diagram of the 3D digital phase encoding model. The incident phase is encoded into different types of transmission phases  $\psi_i$  and  $\psi_i + n\psi_0$ , where  $n$  represents the steps of digitization. (b) Liquid silicone elastomer in the mold (ABS frames) to fabricate the phase encoding body. (c) Silicone elastomer with the same bottom diameter  $W = 42$  mm and different volume fractions  $T(x, y)/H$  were inserted into the background water and the phase is encoded from “0” to “ $2\pi$ ,” respectively. (d) Theoretical phase shift curves with the decreasing of digitization steps.

digital phase encoding is capable of achieving broadband phase modulation.

### III. EXPERIMENTAL VALIDATION OF BROADBAND PHASE ENCODING

Figure 2(a) shows the photograph of the fabricated broadband phase encoding model. The plane-piston transducer with a working frequency from 50 to 500 kHz generated a 5-cycle tune-burst signal with a pulse repetition period of 165 ms. The measured phase profile and relative amplitude near the surface of the plane-piston transducer at the frequency of 100 kHz are shown in Figs. 2(b) and 2(c), respectively. The above two experimental results show that the phase distribution is flat within the

aperture of the transducer, and the amplitude of the acoustic field is gradually decreasing along the radius direction of the transducer. The fabricated phase encoding mold was divided into nine types of measurement regions, and each square region was further divided into another nine regions with equal lengths and widths to facilitate the measurement of phase deflection results statistically. By changing the incident frequency from 100 to 500 kHz, the experimental results show that the incident acoustic phase is encoded from coding bit “0” to “ $2\pi$ .” The experimental phase distributions at the frequencies of 100, 200, 300, 400, and 500 kHz are shown in Figs. 2(e)–2(i), respectively. Figure 2(d) shows measured a line plot of phase deflection with different positions at the frequency from 100 to 500 kHz. Statistically, the experimental results show

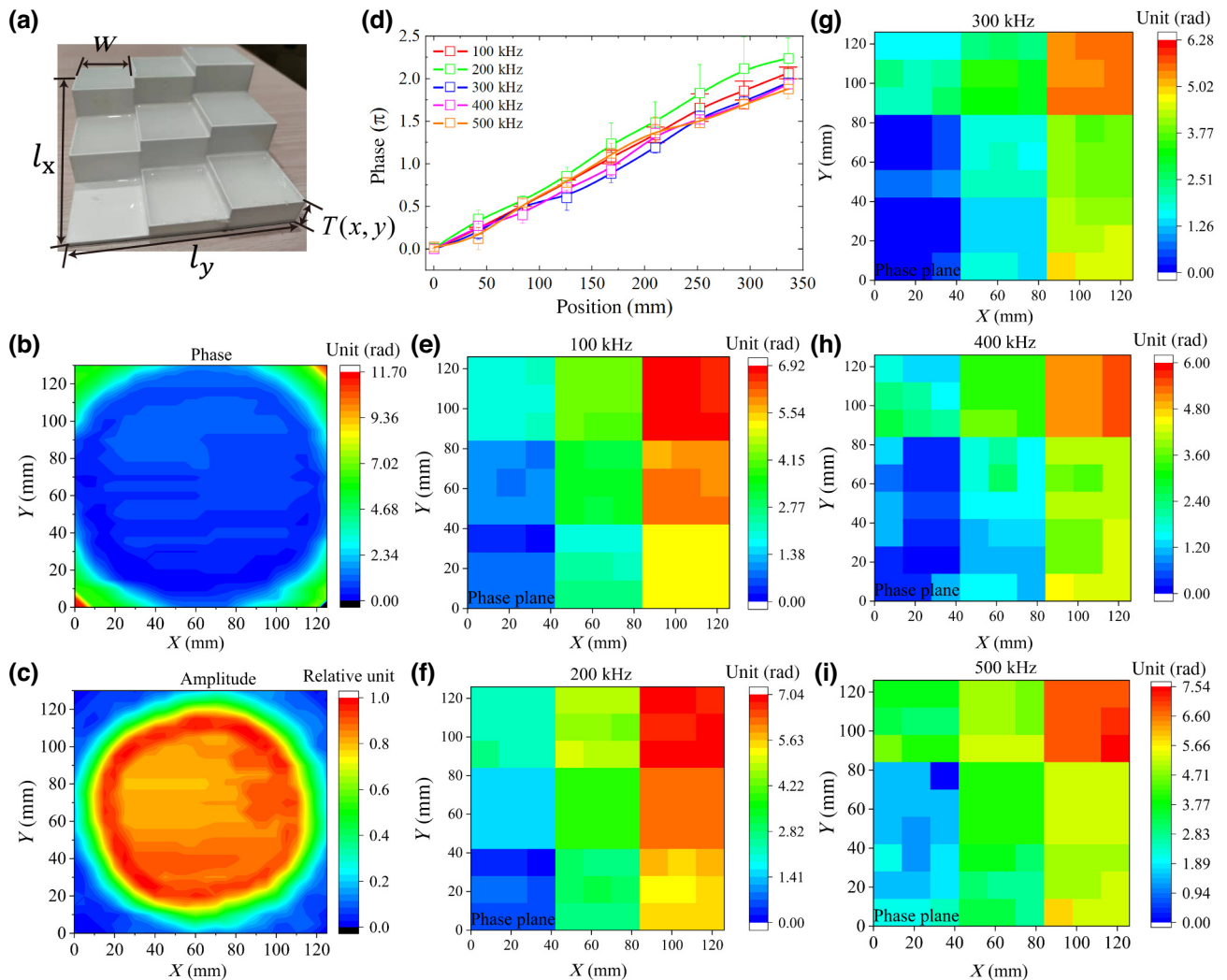


FIG. 2. (a) Photograph of the phase encoding model. (b) Statistically broadband phase deflection performance of the phase encoding. Each phase value in the phase encoding region is measured nine times statistically. (c),(d) The measured acoustic phase and amplitude distributions without phase encoding model at the frequency of 100 kHz. (e)–(i) Measured phase profile with digital phase encoding model at the frequencies of 100, 200, 300, 400, and 500 kHz, respectively, which is divided into nine types of phase encoding regions, respectively.

that broadband digital phase encoding covers the coding bit “0” to “ $2\pi$ .” The received acoustic signals at different encoding positions are phase-normalized from “0” to “ $2\pi$ ,” the received transmission signals in the time domain are shown in supplementary material Fig. S2 [40].

#### IV. DESIGN AND VALIDATION OF SOFT METACOLLIMATOR BY BROADBAND DIGITAL PHASE ENCODING

Based on the above broadband characterization of soft material parameters, we proposed the method of broadband digital phase encoding. In the next part, we will demonstrate the performance of broadband digital phase encoding in the acoustic wave manipulation area including achieving two various soft metacollimator over the broad frequency band. First, the spherical wavefront is expected to be transformed to a plane wavefront using a soft metacollimator fabricated by a broadband digital phase encoding scheme. The spatially varying phase accumulation could achieve aberration-free acoustic collimation if the phase accumulation follows the hyperbolic gradient profile:

$$\psi_{\text{coll}}(r) = \frac{2\pi}{\lambda}(S_0 - \sqrt{d^2 + r^2}), \quad (6)$$

where  $\lambda$  is the wavelength in the background medium of the incident wave,  $d = 50$  mm is the distance between the omnidirectional source and the center of the soft metacollimator,  $S_0 = 4.463T$  is the parameter related to the maximum thickness  $T = 60$  mm of soft metacollimator, and  $r$  is the coordinate along the radius direction of soft metacollimator, where the value of coordinate  $r$  is changing from  $-60$  mm to  $60$  mm. As shown in Fig. 3(a), the three-dimensional soft metacollimator at different frequencies were designed according to Eqs. (1) and (2). According to the principle of our proposed broadband digital phase encoding, the continually accumulated phase profile is required to be discretized for ensuring that the lattice constant of each discrete unit is less than a one-half wavelength. The corresponding accumulated phase profile and discretized method for the soft metacollimator is shown in Fig. 3(b) at the frequency of 50 kHz, 100 kHz, and 300 kHz, respectively. The detailed information of 2D phase profiles on designed soft metacollimators at different frequencies are shown in supplementary material Fig. S2 [40]. From the phase profiles extracted at the surface of the soft metacollimator [Fig. 3(b)], it can be seen that the phase change rate at the radius direction is improved with the increase in frequency. To demonstrate the soft metacollimator by our broadband digital phase encoding could transfer spherical acoustic wavefront to plane acoustic wavefront, we performed finite element simulations with COMSOL MULTIPHYSICS 5.6 (Stockholm, Sweden) as shown in Fig. 3(c). The dynamical parameters

of silicone elastomers including speed of sound is measured as 1027.17 m/s and the density is 1090.53 kg/m<sup>3</sup>. The two different simulation results at frequencies of 50 and 100 kHz clearly reveal the broadband collimation functionality of our soft metacollimator. The fabricated method of soft metacollimator by silicone elastomer is the same as those mentioned in Fig. 2. The point source is placed at 50 mm away from the soft metacollimator and the simulated acoustic pressure field reveals that the point source located at the position  $y = 0$  is converted into the plane wave at the position  $y = 6\lambda_0$  by the soft metacollimator.

In order to verify the features of our designed soft metacollimator by broadband digital phase encoding, we discretized two kinds of soft metacollimator with continuous phase distributions (see detailed information in supplementary material Fig. S3 [40]) by phase encoding technique. Underwater acoustic experiments were performed in a high-intensity anechoic water tank with dimensions of 2 m  $\times$  1.2 m  $\times$  0.8 m. The schematic diagram of the experimental setup is shown in supplementary material Fig. S4 [40]. The designed soft metacollimator was submerged at the center of the water tank. The five-cycle tone burst signal from 50 to 200 kHz with a trigger interval of 165 ms is generated using a functional signal generator (AFG 31000 SERIES; Tektronix). The signal is next amplified by a broadband power amplifier and drives a 27-mm-diameter spherical source to transmit the broadband acoustic signals. Changing the input resistance value of the power amplifier makes the input voltage of the transducer change from 5 to 170 V. A broadband hydrophone (RSHA-10; Receiving Sensitivity:  $-210$  dB) with the acoustic a center diameter of 13 mm and a length of 67.5 mm is driven by dc regulated power supply to record acoustic signals during motor scanning. Sound pressure field  $P(x, y)$  and  $P_0(x, y)$  in the presence and absence of a soft metacollimator is measured at a sampling rate of 1.25 MHz. The 3D mobile motor with a minimum accuracy of 1 mm has been used for sound field scanning experiments to ensure the spatial resolution was 30 times higher than the incident wavelength (30 mm) at the working frequency of 50 kHz. The signals are acquired via a digital oscilloscope (MDO32; Tektronix), and then converted and processed on a computer. The duration of the incident pulses is about 80  $\mu$ s which is short enough to isolate reflections from the tank walls (supplementary materials Fig. S5 [40]). Photographs of the designed soft metacollimator at different frequencies are shown on the right of supplementary material Fig. S4 [40].

Measurements of soft metacollimator are performed in the  $x$ - $y$  plane over a broad range of frequencies from 50 to 100 kHz, respectively. As shown in Fig. 4(a), the spherical wavefront is modulated to plane wavefront by soft metacollimator, the simulated diffraction distance from  $6\lambda_0$  to  $27\lambda_0$  is outlined by a white dashed line for comparing the

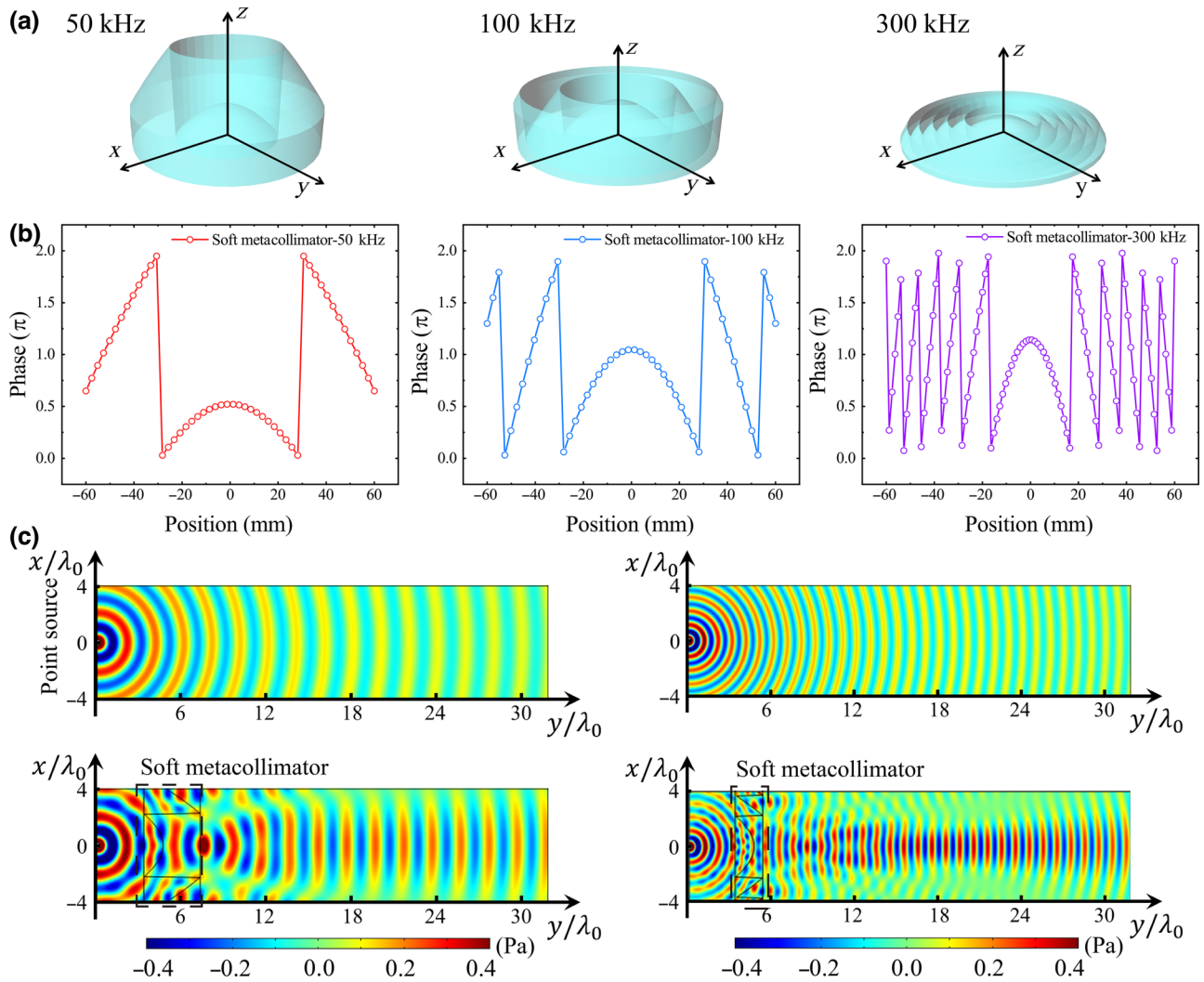


FIG. 3. (a) The soft metacollimator models in different frequencies of 50, 100, and 300 kHz, respectively. (b) The phase profile includes the soft metacollimator at frequencies of 50, 100, and 300 kHz, respectively. (c) Simulated acoustic pressure field of the soft metacollimator at 50 and 100 kHz. The spherical wavefront is converted into a plane wavefront capable of acoustic directional emission.

experimental results [Fig. 4(b)]. As shown in Fig. 4(c), simulated and measured sound pressure field along  $x = 0$  and  $y = 12\lambda_0$  direction is normalized by the maximum sound pressure point at  $(0, 0)$  and  $(0, 12\lambda_0)$ , respectively. The experimental normalized main lobe amplitude along  $y = 12\lambda_0$  is improved from 62.7% to 100%, which show good agreements with predictions. In addition, we also extracted the frequency response curve of sound pressure level (SPL) gain and full width at half maximum (FWHM) at frequencies from 50 to 500 kHz. For a quantitative analysis of the acoustic collimation properties of the designed soft metacollimator by broadband digital phase encoding, the red solid curve (red hollow circles) and red triangle in Fig. 4(d) show the simulated and measured SPL and FWHM in the presence of soft metacollimator, respectively. The measured SPL is improved by about 7.63 and

7.77 dB at frequencies of 50 and 100 kHz in agreement with the simulation results. Furthermore, the measured FWHM (red solid circle) is 50 and 40 mm at frequencies of 50 and 100 kHz, respectively, compared with 500 and 460 mm without the soft metacollimator. Simulations and experimental results both indicate more than ten times spatial resolution by introducing the soft metacollimator.

## V. LONG-DISTANCE TRANSMISSION AND BROADBAND PERFORMANCES OF SOFT METACOLLIMATOR

The broadband digital phase encoding properties and energy enhancement performance of the acoustic soft metacollimator are investigated by underwater long-distance transmission experiments. The experiment was

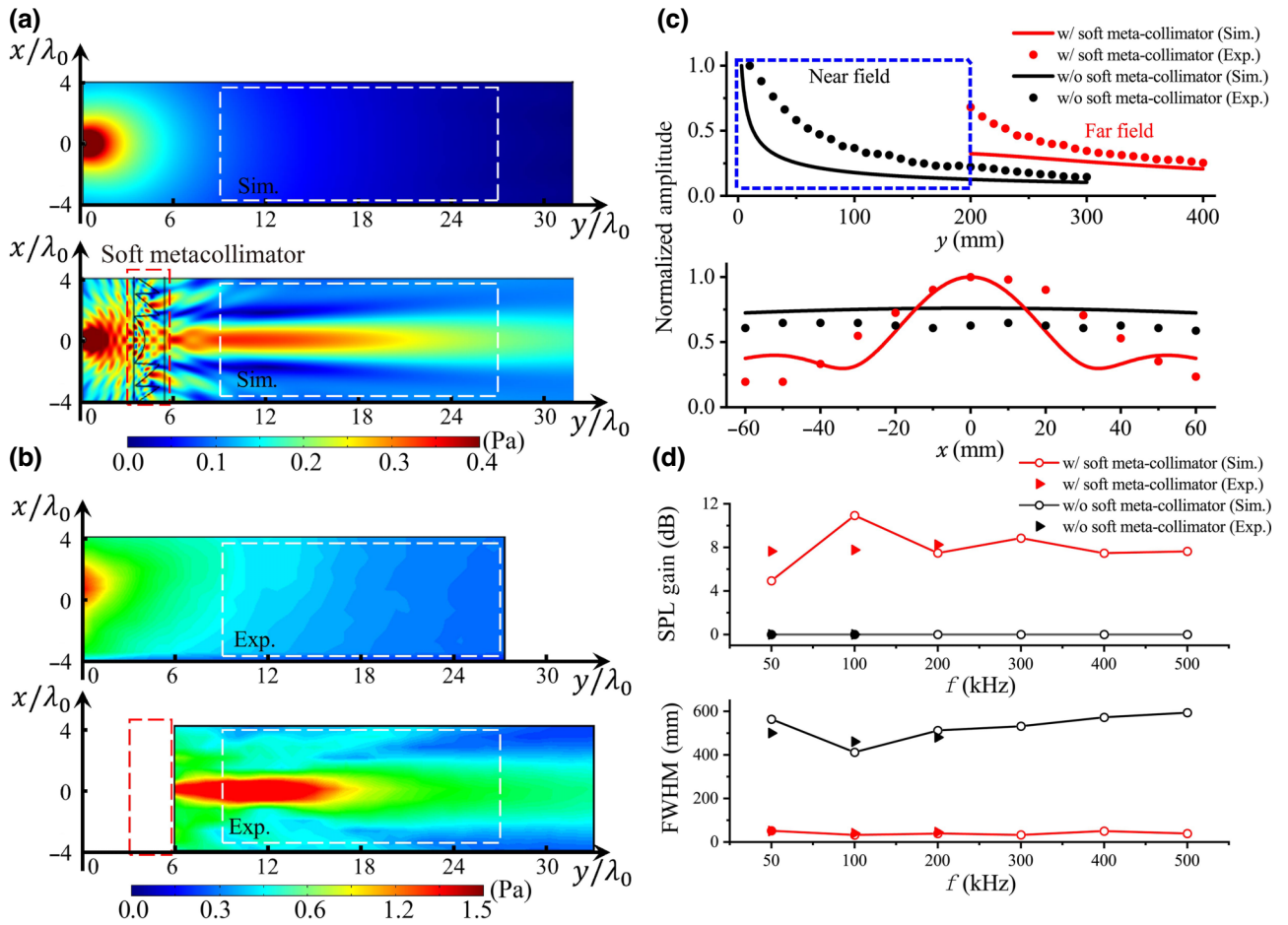


FIG. 4. (a) Simulation results that a spherical wave is modulated to a plane wave by a soft metacollimator at a frequency of 100 kHz. (b) Experimental acoustic pressure fields correspond to the simulation results, in which the white dashed line indicates the same region with simulations. (c) Comparison of an empty field and sound pressure field with soft metacollimator along  $x = 0$  and main lobe along  $y = 12\lambda_0$ . (d) Sound pressure level (SPL) gain and full width at half maximum (FWHM) in the presence and absence of the soft metacollimator at frequencies from 50 to 500 kHz.

conducted in a water tank with dimensions of 27 m in length, 15 m in width, and 5 m in depth. Based on a rough estimation, even for the lowest 50 kHz sound wave excitation, the wavelength in the medium is approximately 30 mm. In the length, width, and depth directions, this allows for approximately 900, 500, and 166 wavelengths to be covered, respectively. These experimental conditions ensure that five sinusoidal pulses can be strictly separated in the time domain from the transducer port to the hydrophone receiver. The pulse width is approximately 150 mm at 50 kHz. Such experimental conditions guarantee that the reverberation field does not significantly affect the estimation of the direct signal, even in the absence of sound-absorbing panels. As illustrated in Figs. 5(a) and 5(b), two kinds of soft metacollimators are placed between the underwater detection system and background water. At the frequency from 60 to 110 kHz, metacollimator 1 with a low cutoff frequency of 50 kHz has been used for energy

enhancement, and metacollimator 2 with a low cutoff frequency of 100 kHz has been used from 110 to 150 kHz, respectively. As shown in Figs. 5(c) and 5(d), with the introduction of two different soft metacollimators, the transmission voltage has been improved over two times at the distance of a 16 m. The broadband digital phase encoding properties of the soft metacollimator are also studied by broadband encoding experiments. As shown in Fig. 5(e), we compared the transmission SPL gain of our designed soft metacollimators at different frequencies and distances. By comparing the frequency responses at a distance of 8 m, soft metacollimator 1 could obtain an 8–10 dB SPL gain over a low cutoff frequency of 50 kHz [Fig. 5(f)], while soft metacollimator 2 could achieve a gain of 3–8 dB over a low cutoff frequency of 100 kHz [Fig. 5(g)], respectively. The results in Fig. 5(f) clearly demonstrate the SPL gain above the low cutoff frequency range. This indicates that customizable soft metacollimators with adjustable cutoff

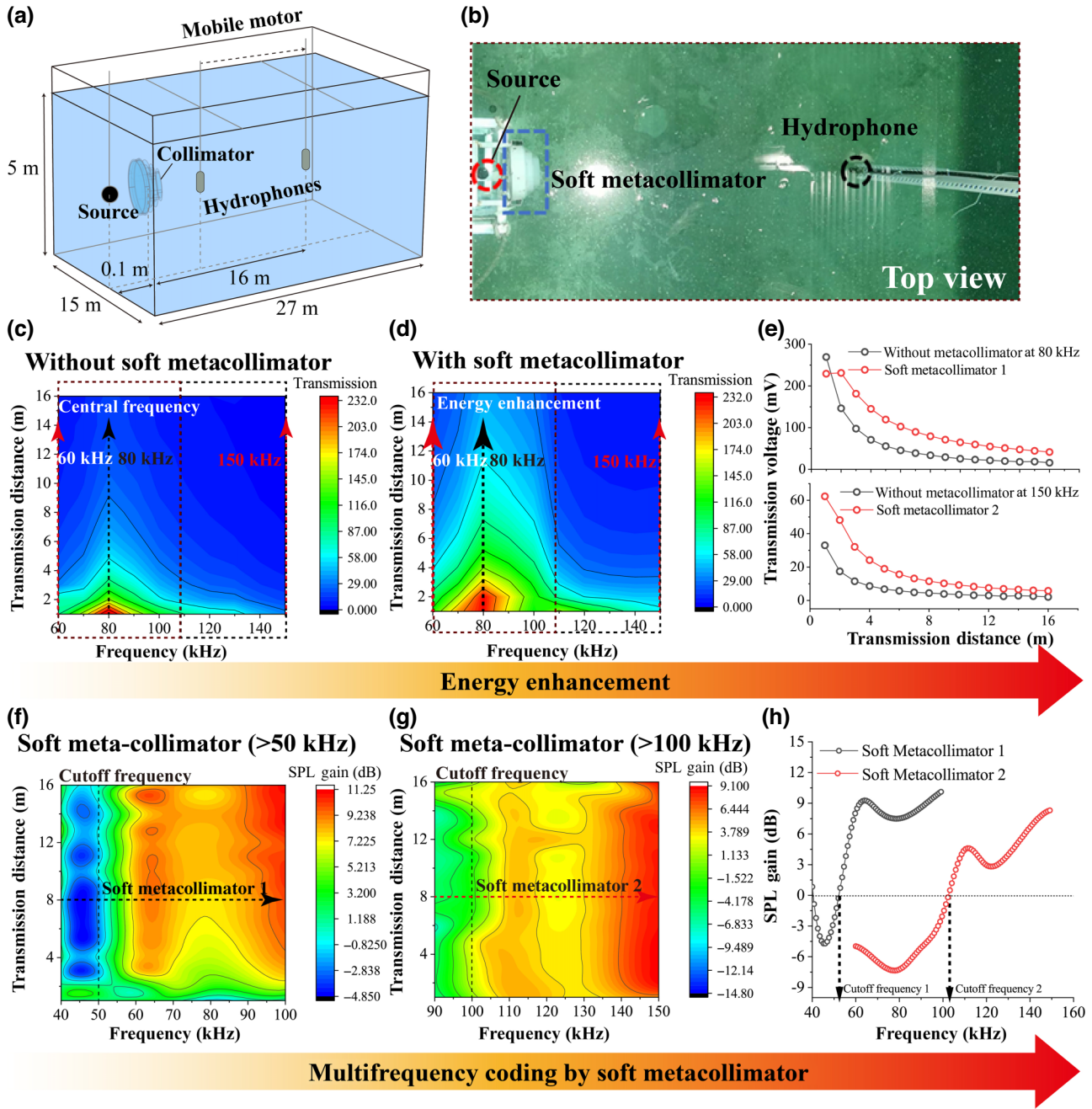


FIG. 5. (a),(b) Energy enhancement at distances from 0 to 16 m without and with soft metacollimator. (c) Comparison of transmission voltage at frequencies of 80 and 100 kHz. (d),(e) broadband coding properties of soft metacollimator at frequencies above 50 and 100 kHz, respectively. (f) broadband gain of sound pressure level (SPL) with two kinds of soft metacollimators.

frequency can obtain a wideband gain in SPL above its low cutoff frequency.

### VI. CONCLUSION

In summary, we have proposed and experimentally demonstrated an acoustic soft metacollimator based on a novel broadband digital phase encoding. Initially, we elucidated on the mechanism of phase encoding by adjusting the

volume fractions of water within soft silicone elastomers. Subsequently, we fabricated the digital phase encoding models experimentally, achieving a linear changing phase profile and observing a broadband performance spanning from 50 to 500 kHz. Utilizing the unique properties of the phase encoding, we designed two kinds of soft metacollimator, which enhanced the transmission intensity by 7.7 dB and improved the spatial resolution tenfold. The phase modulation capability of the acoustic soft metacollimator



is able to convert spherical wavefront to plane wavefront at different frequencies. Moreover, the proposed phase encoding provides intuitive modulation of arbitrary wavefronts including focused spherical wavefront, helical wavefront, and the holographic wavefront. Theoretically, phase encoding based on soft materials offers a higher degree of freedom and controllability than rigid materials, the phase tunability and impedance matching of soft tunable elastomers allow for more possibilities. It is worth noting that the theoretical analysis is based on the high-frequency approximation  $\nabla A^2/A \ll k^2$ . With decreasing frequency, the imaginary part of Eq. (1) satisfies

$$\frac{2\nabla A}{A} \cdot \nabla \varphi(\mathbf{r}) + \nabla^2 \varphi(\mathbf{r}) = 0. \quad (7)$$

Through a meticulous derivation process, it has become evident that the phase of the sound pressure in the eikonal equation is solely contingent upon the refractive index

$$\frac{d}{ds} \nabla \varphi = \nabla n(\mathbf{r}, z). \quad (8)$$

However, in scenarios where the consideration of intensity contribution becomes necessary, it becomes imperative to calculate the intensity function

$$\nabla \cdot (A^2 \nabla \varphi) = 0. \quad (9)$$

After introducing an abrupt phase shift at the interface between two different mediums, the laws of reflection and refraction by applying Fermat's principles have been revisited [41]. In our proposed phase coding theory, we introduced a gradient refractive index that can lead to local phase changes that is similar to the generalized Snell's law. However, the generalized Snell's law does not actually consider much about the intensity function, which provide more freedom to control energy across two different interfaces. Furthermore, the soft material encoding system we propose is a novel impedance matching system. In a simple estimation, the current speed of sound in soft materials is approximately 1000 m/s. With the same pixel density, the thickness of our designed device (twice the wavelength, approximately 40 mm) is reduced by at least half compared with the processing thickness (80 mm) mentioned in most 3D printed metamaterials at a frequency of 50 kHz. Therefore, it provides greater freedom for lightweight and miniaturized applications (Fig. S6 in the supplementary material [40]).

It is important to note that for an individual soft metacollimator device, the operating frequency is not strictly broadband. It has a minimum cutoff frequency and is fundamentally limited by the narrowband transducer. However, when the operating bandwidth is from 50 to 500 kHz, the metacollimators show the broadband performance in waveform modulation and collimation.

In conclusion, this new broadband digital phase encoding technology may pave a new route for future acoustic functional devices such as programmable helical wave communicators, acoustic microscopes, acoustic tweezers, acoustic antennas, and holographic projectors. The data that support the findings of this study are available from the corresponding author upon reasonable request.

## ACKNOWLEDGMENTS

This work was supported by the National Natural Science Foundation of China (Grant No. 12074323), Special Fund for Marine and Fishery Development of Xiamen (Grant No. 20CZB015HJ01), Water Conservancy Science and Technology Innovation Project of Guangdong (Grant No. 2020-16), and Major Science and Technology Project of Fujian (Grant No. 2021NZ033016), China National Postdoctoral Program for Innovative Talents (Grant No. BX2021168), China Postdoctoral Science Foundation (Grant No. 2020M682086), National Science Foundation of Fujian Province of China (No. 2022J02003), National Natural Science Foundation of China (Grant No. 62271235), Doctoral Scientific Research Foundation of Liaoning Province (Grant No. 2021-BS-019), and Jockey Club Trust (Grant number GSP181) STEM Lab of Scalable and Sustainable Photonic Manufacturing in the University of Hong Kong. We also want to thank Jiali Huang for the helpful assistance in experiments.

- 
- [1] J. B. Pendry, A. J. Holden, W. J. Stewart, and I. Youngs, Extremely low frequency plasmons in metallic mesostructures, *Phys. Rev. Lett.* **76**, 4773 (1996).
  - [2] J. B. Pendry, A. J. Holden, D. J. Robbins, and W. J. Stewart, Magnetism from conductors and enhanced non-linear phenomena, *IEEE Trans. Microw. Theory Tech.* **47**, 2075 (1999).
  - [3] R. A. Shelby, D. R. Smith, and S. Schultz, Experimental verification of a negative index of refraction, *Science* **292**, 77 (2001).
  - [4] S. A. Cummer, J. Christensen, and A. Alù, Controlling sound with acoustic metamaterials, *Nat. Rev. Mater.* **1**, 16001 (2016).
  - [5] H. Ge, M. Yang, C. Ma, M. H. Lu, Y. F. Chen, N. Fang, and P. Sheng, Breaking the barriers: advances in acoustic functional materials, *Natl. Sci. Rev.* **5**, 159 (2018).
  - [6] A. M. Shaltout, V. M. Shalaev, and M. L. Brongersma, Spatiotemporal light control with active metasurfaces, *Science* **364**, eaat3100 (2019).
  - [7] J. Liu, W. Wang, C. Zhao, Y. Zhou, H. Zhang, B. Liang, C.-W. Qiu, and J.-C. Cheng, Static passive meta-sonar for dynamic sound beam scanning, *Sci. Bull.* **68**, 1862 (2023).
  - [8] J. Liu, Z. Li, B. Liang, J.-C. Cheng, and A. Alù, Remote water-to-air eavesdropping with a phase-engineered impedance matching metasurface, *Adv. Mater.* **35**, 2301799 (2023).

- [9] Y. Xie, W. Wang, H. Chen, A. Konneker, B. I. Popa, and S. A. Cummer, Wavefront modulation and subwavelength diffractive acoustics with an acoustic metasurface, *Nat. Commun.* **5**, 5553 (2014).
- [10] N. Fang, D. Xi, J. Xu, M. Ambati, W. Srituravanich, C. Sun, and X. Zhang, Ultrasonic metamaterials with negative modulus, *Nat. Mater.* **5**, 452 (2006).
- [11] G. W. Milton, M. Briane, and J. R. Willis, On cloaking for elasticity and physical equations with a transformation invariant form, *New J. Phys.* **8**, 248 (2006).
- [12] M. Farhat, S. Enoch, S. Guenneau, and A. B. Movchan, Broadband cylindrical acoustic cloak for linear surface waves in a fluid, *Phys. Rev. Lett.* **101**, 134501 (2008).
- [13] B. I. Popa, L. Zigoneanu, and S. A. Cummer, Experimental acoustic ground cloak in air, *Phys. Rev. Lett.* **106**, 253901 (2011).
- [14] Z. Chen, Y. Peng, H. Li, J. Liu, Y. Ding, B. Liang, X. F. Zhu, Y. Lu, J. Cheng, and A. Alù, Efficient nonreciprocal mode transitions in spatiotemporally modulated acoustic metamaterials, *Sci. Adv.* **7**, eabj1198 (2021).
- [15] N. Kaina, F. Lemoult, M. Fink, and G. Lerosey, Negative refractive index and acoustic superlens from multiple scattering in single negative metamaterials, *Nature* **525**, 77 (2015).
- [16] K. Melde, A. G. Mark, T. Qiu, and P. Fischer, Holograms for acoustics, *Nature* **537**, 518 (2016).
- [17] Y. Ding, Z. Liu, C. Qiu, and J. Shi, Metamaterial with simultaneously negative bulk modulus and mass density, *Phys. Rev. Lett.* **99**, 093904 (2007).
- [18] E. Bok, J. J. Park, H. Choi, C. K. Han, O. B. Wright, and S. H. Lee, Metasurface for water-to-air sound transmission, *Phys. Rev. Lett.* **120**, 044302 (2018).
- [19] T. Li, G. Li, Y. Liang, T. Cheng, J. Dai, X. Yang, B. Liu, Z. Zeng, Z. Huang, Y. Luo, T. Xie, and W. Yang, Fast-moving soft electronic fish, *Sci. Adv.* **3**, e1602045 (2017).
- [20] Q. Zhong, J. Zhu, F. E. Fish, S. J. Kerr, A. M. Downs, H. Bart-Smith, and D. B. Quinn, Tunable stiffness enables fast and efficient swimming in fish-like robots, *Sci. Robot.* **6**, eabe4088 (2021).
- [21] Y. Gao, J. Song, S. Li, C. Elowsky, Y. Zhou, S. Ducharme, Y. M. Chen, Q. Zhou, and L. Tan, Hydrogel microphones for stealthy underwater listening, *Nat. Commun.* **7**, 12316 (2016).
- [22] H. S. Wang, S. K. Hong, J. H. Han, Y. H. Jung, H. K. Jeong, T. H. Im, C. K. Jeong, B. Y. Lee, G. Kim, C. D. Yoo, and K. J. Lee, Biomimetic and flexible piezoelectric mobile acoustic sensors with multiresonant ultrathin structures for machine learning biometrics, *Sci. Adv.* **7**, eabe5683 (2021).
- [23] P. Jin, J. Fu, F. Wang, Y. Zhang, P. Wang, X. Liu, Y. Jiao, H. Li, Y. Chen, Y. Ma, and X. Feng, A flexible, stretchable system for simultaneous acoustic energy transfer and communication, *Sci. Adv.* **7**, eabg2507 (2021).
- [24] T. Brunet, A. Merlin, B. Mascaró, K. Zimny, J. Leng, O. Poncelet, C. Aristégui, and O. Mondain-Monval, Soft 3D acoustic metamaterial with negative index, *Nat. Mater.* **14**, 384 (2015).
- [25] E. Dong, Z. Song, Y. Zhang, S. G. Mosanenzadeh, Q. He, X. Zhao, and N. X. Fang, Bioinspired metagel with broadband tunable impedance matching, *Sci. Adv.* **6**, eabb3641 (2020).
- [26] K. Zhang, C. Ma, Q. He, S. Lin, Y. Chen, Y. Zhang, N. X. Fang, and X. Zhao, Metagel with broadband tunable acoustic properties over air–water–solid ranges, *Adv. Funct. Mater.* **29**, 1903699 (2019).
- [27] A. Ba, A. Kovalenko, C. Aristégui, O. Mondain-Monval, and T. Brunet, Soft porous silicone rubbers with ultra-low sound speeds in acoustic metamaterials, *Sci. Rep.* **7**, 40106 (2017).
- [28] Y. Li, B. Liang, Z. M. Gu, X. Y. Zou, and J. C. Cheng, Reflected wavefront manipulation based on ultrathin planar acoustic metasurfaces, *Sci. Rep.* **3**, 2546 (2013).
- [29] K. Tang, C. Qiu, M. Ke, J. Lu, Y. Ye, and Z. Liu, Anomalous refraction of airborne sound through ultrathin metasurfaces, *Sci. Rep.* **4**, 6517 (2014).
- [30] Y. Li, X. Jiang, B. Liang, J. C. Cheng, and L. Zhang, Metascreen-based acoustic passive phased array, *Phys. Rev. Appl.* **4**, 024003 (2015).
- [31] Y. Zhu, X. Fan, B. Liang, J. Cheng, and Y. Jing, Ultrathin acoustic metasurface-based Schroeder diffuser, *Phys. Rev. X* **7**, 021034 (2017).
- [32] H. Zhang, W. Zhang, Y. Liao, X. Zhou, J. Li, G. Hu, and X. Zhang, Creation of acoustic vortex knots, *Nat. Commun.* **11**, 3956 (2020).
- [33] X. Zhu, K. Li, P. Zhang, J. Zhu, J. Zhang, C. Tian, and S. Liu, Implementation of dispersion-free slow acoustic wave propagation and phase engineering with helical-structured metamaterials, *Nat. Commun.* **7**, 11731 (2016).
- [34] Z. Chen, C. Xue, L. Fan, S. Y. Zhang, X. J. Li, H. Zhang, and J. Ding, A tunable acoustic metamaterial with double-negativity driven by electromagnets, *Sci. Rep.* **6**, 30254 (2016).
- [35] Y. Zhu, L. Cao, A. Merkel, S. W. Fan, B. Vincent, and B. Assouar, Janus acoustic metascreen with nonreciprocal and reconfigurable phase modulations, *Nat. Commun.* **12**, 7089 (2021).
- [36] A. Özcelik, J. Rufo, F. Guo, Y. Gu, P. Li, J. Lata, and T. J. Huang, Acoustic tweezers for the life sciences, *Nat. Methods* **15**, 1021 (2018).
- [37] C. Shi, M. Dubois, Y. Wang, X. Zhang, and P. Sheng, High-speed acoustic communication by multiplexing orbital angular momentum, *Proc. Natl. Acad. Sci. USA* **114**, 7250 (2017).
- [38] E. Dong, P. Cao, J. Zhang, S. Zhang, N. X. Fang, and Y. Zhang, Underwater acoustic metamaterials, *Natl. Sci. Rev.* **10**, nwac246 (2023).
- [39] J. Zhang, T. Zhang, E. Dong, C. Zhang, Z. Lin, Z. Song, H. Li, N. X. Fang, and Y. Zhang, Bioinspired hydrogel jellyfish with mechanical flexibility and acoustic transparency, *Cell Rep. Phys. Sci.* **3**, 101081 (2022).
- [40] See Supplemental Material at <http://link.aps.org/supplemental/10.1103/PhysRevApplied.22.014065> for the details on measured phase profile, time-domain diagram, design and discrete phase distribution, experimental setup in a water tank, and applications.
- [41] N. Yu, P. Genevet, M. A. Kats, F. Aieta, J.-P. Tetienne, F. Capasso, and Z. Gaburro, Light propagation with phase discontinuities: generalized laws of reflection and refraction, *Science* **334**, 333 (2011).